POLYSACCHARIDIC-POLYDOPAMINE BEADS TOWARDS NEXT-GENERATION OF CELL ENCAPSULATION: A COMPOSITIONAL STUDY

Andreea Ioana DINU [1], Maria-Ruxandra SMARANDI[2], Cristina STAVARACHE[1], Alexandra MOCANU-DOBRANICI[3], Sorina DINESCU[3], Adriana LUNGU[1], Elena OLAREȚ[1], Horia IOVU[1*]

Investigating the optimal formulation for polysaccharidic–polydopamine beads is essential to improving cell encapsulation technologies because it directly affects key attributes including porosity, surface bioactivity, crosslinking density, and degradation rate. While polydopamine (PDA) adds adhesive and functional groups that can improve cell-matrix interfaces and support structural integrity, alginate and pectin provide a gentle and physiologically acceptable framework for cell encapsulation. In this work, we investigate the effects of several PDA inclusion techniques in the polymeric matrix on the physico-chemical and biological characteristics, which together dictate the survivability and proliferation of encapsulated cells. For tissue engineering and long-term cell-based treatment applications, this compositional adjustment is especially requisite.

Keywords: polydopamine, polysaccharide, hydrogel composite beads

1. Introduction

In recent years, the development of advanced cell encapsulation systems has become pivotal for engineering physiologically relevant 3D microenvironments. In order to preserve normal cell growth, gene expression, and cellular functions, 3D cell culture is now acknowledged as a superior alternative technique *in vitro* when compared to conventional 2D plate culture. This is because it can produce a cellular microenvironment that replicates the interactions between cells and the extracellular matrix (ECM). There are the two primary categories into which 3D cell culturing systems are often divided: scaffold free and scaffold-based. Among these, the latter is frequently better suited for *in vitro* cell culture since it provides a more physiologically relevant environment while simultaneously shielding cells

* Corresponding author, Horia Iovu, e-mail: horia.iovu@upb.ro
[1] Advanced Polymer Materials Group, Faculty of Chemical Engineering and Biotechnology, National University of Science and Technology "POLITEHNICA", Bucharest, Romania, e-mail: andreea_ioana.dinu@upb.ro, adriana.lungu@upb.ro, cristina.stavarache@upb.ro, elena.olaret@upb.ro,
[2] Faculty of Medical Engineering, National University of Science and Technology "POLITEHNICA", Bucharest, Romania, e-mail: maria.smarandi@stud.fim.upb.ro
[3] Department of Biochemistry and Molecular Biology, University of Bucharest, Romania, e-mail: dobranici.alexandra-elena@s.bio.unibuc.ro, sorina.dinescu@bio.unibuc.ro

from environmental stress and promoting migration of cells, propagation, and differentiation [1].

Natural polymer-based bead scaffolds have sparked notable interest due to their superior porosity, facilitating efficient diffusion of nutrients and metabolic byproducts; their large surface area, promoting enhanced cell adhesion; and their exceptional biological compatibility, rendering them ideal for cell cultivation and tissue modeling applications [2]. Proteins such as gelatin or collagen are commonly used due to their natural cell-binding ligands, but they pose challenges such as batch-to-batch variability, limited availability, potential immunogenicity, and the risk of pathogen transmission. On the other hand, plant-based polysaccharides offer better biocompatibility and mild gelation conditions, but special attention should be paid to compositional variability, mechanical properties, and gelation tunability [3]. Among natural polymers there have been reports of glucomannan [4], cellulose [5] and alginate [6] beads as successful cell-encapsulation matrices. The most notable of all, alginate-based hydrogel beads have been extensively reported as encapsulation matrix for many types of cells (mesenchymal stem cells - MSCs [7], cancer stem cells [8]) due to their easy preparation and tunable biophysical properties. However, polymeric systems containing alginate alone can exhibit disadvantages such as poor mechanical properties and rapid degradation, which are reasons for incorporation of other polysaccharides, such as pectin. Pectin is also a natural polysaccharide that possesses a backbone abundant in negatively charged carboxyl groups. These groups can engage in calcium ion (Ca^{2+})-mediated crosslinking with alginate chains, leading to the establishment of a stable and resilient hydrogel network [9]. Nonetheless, alginate has limited cell adhesiveness owing to its inadequate protein adsorption resulting from its hydrophilic characteristics [10]. Several ways have been implemented to improve cell anchoring and interaction inside alginate gel. For instance, alginate was altered with peptides including an RGD sequence to enhance cell survival, including cell adhesion, migration, and differentiation [11]. From another perspective, dopamine (DA), acknowledged as an essential neurotransmitter in the central nervous system which is conventionally examined for its function in modulating emotion, motion, and incentive pathways, has discovered an intriguing and unanticipated vocation: biomaterial engineering [12]. This metamorphosis across disciplines, from neuroscience to material engineering, showcases dopamine's structural versatility and functional complexity, qualities now being utilized to address enduring issues in 3D cell cultures. A significant development occurred when it was shown that dopamine has the ability to self-polymerize in an alkaline environment. This process produces PDA nanoparticles that resemble the adhesive proteins of mussels and exhibits remarkable adherence to various surfaces. Furthermore, the polymeric form of dopamine provides a veritable trove of functional groups, including catechol, amines, and imines, which facilitate conjugation with biomolecules that,

in turn, increase cell attachment [13]. PDA has superior biodegradability and limited cytotoxicity, both of which are essential for its medical applications [14], as well as reactive oxygen species (ROS) scavenging ability that is very useful for protecting encapsulated cells [15]. PDA-integrating advanced 3D cell culture models have gained a lot of interest lately, mainly exploiting the beneficial effects of PDA coatings on various materials to enhance cell adhesion and proliferation [16]. By combining the cell-adhesive behavior of PDA with the biological suitability and biodegradability of both alginate and pectin, a viable approach to the development of sophisticated 3D cell culture environments is envisioned.

In the present study, three distinct approaches for incorporating PDA into a polysaccharide matrix will be explored: (i) in situ polymerization of DA grafted onto the alginate backbone, (ii) in situ polymerization of DA monomers, and (iii) physical mixing of pre-synthesized PDA particles [17].

(i) Activating compounds like NHS (N-hydroxysuccinimide) and EDC (1-ethyl-3-(3-dimethylaminopropyl)carbodiimide) are used to chemically couple alginate with DA [18].

(ii) Grafted DA can polymerize in alkaline conditions to generate PDA either within the polymeric matrix or as a shell on beads [19].

(iii) PDA particles can be obtained by self-oxidative polymerization of dopamine separately and their inclusion in the polymeric blend was found to exhibit excellent cell attachment [20].

To the best of our knowledge, no study has reported so far the comparison between all three distinct incorporation methods of PDA in a polysaccharidic matrix. Additionally, combining these bioinspired materials is advantageous since they are all hydrophilic and the resulting solution can be processed into various shapes (beads, fibers, particles) through many fabrication techniques (extrusion, spray-drying, electrospinning). The material composition of the polymeric network, the amount of calcium ions employed for crosslinking, and the presence of other components, including PDA particles, can all affect the dimensions, shape, mechanical properties, stability, and physicochemical characteristics of gel particles [21]. In this study, we engineered a series of formulations using an alginate-pectin polymeric matrix supplemented with PDA, which were processed via injection-gelation method to form macroscopic particles. These beads were comprehensively characterized to assess how the PDA incorporation strategy influences their structural and functional properties. Our goal is to determine the most effective formulation for advancing these polymeric beads as promising cell encapsulation materials.

2. Experimental data

2.1 Materials: Dopamine hydrochloride, sodium alginate from brown algae, 25% ammonium hydroxide, calcium chloride ≥93.0% (anhydrous, granular,

≤7 mm), high methoxyl pectin (DE% = 70–75) from apple, sodium hydroxide 98% (pellets), hydrochloric acid ACS grade 37%, 1-ethyl-(dimethylaminopropyl) carbodiimide (EDC), N-hydroxysulfosuccinimide (NHS), tris(hydroxymethyl)aminomethane (Tris), and absolute ethanol were supplied by Sigma-Aldrich.

2.2 Methods

Alginate functionalization with dopamine. The grafting of DA on alginate's backbone was realized following a protocol described in [22]. Briefly, an alginate solution was prepared in distilled water with a 1% concentration, with its pH adjusted to 4.5–5.5 using 0.1 M HCl. Subsequently, 5 mmol of EDC and NHS were added to the solution and stirred magnetically for 45 minutes. Then, dopamine hydrochloride was added to the mixture and left under stirring overnight at room temperature in a nitrogen atmosphere. The modified alginate was precipitated from solution with ethanol and washed several times. The resulting precipitate constitutes the dopamine-grafted alginate and will be referred to as Alg-DA.

Low-methoxyl pectin synthesis. Highly methoxylated pectin (HMP) was chemically demethylesterified to obtain low methoxylated pectin (LMP) using an alkaline saponification method described in literature [23]. LMP with a degree of methylesterification varying between 12% and 25% was obtained, according to previous research [23].

PDA particles synthesis. This step was performed according to a well-established protocol [20]. To ensure an alkaline environment that favors DA oxidation, a mixture of ammonia solution, ethanol and water was first prepared. A 5% dopamine hydrochloride aqueous solution was added to the above mixture solution dropwise After the reaction was carried out at 30 °C for 24 hours, PDA particles precipitated from the solution. The suspension was centrifuged at 9000 rpm for 30 minutes, and the precipitate was washed three times with distilled water. The collected particles were then dried at 80 °C for 4 hours.

PDA-containing alginate-pectin calcium composite beads. The previously synthesized raw materials (Alg-DA, LMP, and PDA) were used to generate composite spherical particles in a $CaCl_2$ solution by extruding through a needle, with variations depending on the method of PDA incorporation and the type of alginate used (native or functionalized). Table 1 summarizes the composition of each type of obtained material and the morphology of the resulting composites.

Table 1

Composition of materials used in the formation of composite beads

Sample code	**Alg**	**Alg-DA**	**LMP**	**PDA integration**
AL	X		X	-
ADL		X	X	
AL-PDA1	X		X	PDA incorporation

ADL-PDA1		X	X	
AL-PDA2	X		X	PDA shell from dopamine
ADL-PDA2		X	X	
AL-Tris	X		X	-
ADL-Tris-PDA		X	X	PDA in situ generated

To prepare the beads, a solution of Alg or Alg-DA (2%) and LMP (1%) was made with distilled water under magnetic stirring at 40ºC. For AL-PDA1 and ADL-PDA1, PDA particles (0.1%) were added to the polysaccharidic mixture which is then ultrasonicated to ensure an even dispersion of PDA particles. For AL-PDA2 and ADL-PDA2, the extruded beads were introduced in a dopamine solution in Tris 10mM with pH=8 for 6 hours to allow the formation of a PDA layer on their surface. For AL-Tris and ADL-Tris-PDA, Alg or Alg-DA and LMP were dissolved in Tris 10 mM with pH=8 under magnetic stirring at room temperature for 24 to allow for the grafted dopamine to polymerize in PDA. Control beads without PDA (AL and ADL) were also produced by the dissolution of Alg or Alg-DA and LMP in distilled water at room temperature. The polymeric blends of all compositions were extruded using a 0.7 mm needle at a flow rate of 10 mL/h into 1.1% $CaCl_2$ solution and allowed to crosslink for 30 minutes. The resulting spheres were washed with distilled water to remove residual $CaCl_2$, filtered, and lyophilized for 24 hours.

2.3 Characterization methods

2.3.1 Characterization of Alg-DA and PDA particles

Structural analysis was performed using a Bruker VERTEX 70 FTIR-ATR spectrometer (Bruker, Billerica, MA, USA) equipped with a Germanium (Ge) crystal. The spectra of the dried samples were recorded in the wavelength range of 400–4000 cm^{-1}, with 32 scans per sample. UV-Vis measurements were conducted at 25 °C, and the spectra were recorded in the wavelength range of 230–500 nm using a UV-3600 Shimadzu spectrophotometer. ^{1}H-NMR spectra of the raw materials were recorded using a Bruker Avance 500 MHz spectrometer. The degree of functionalization (DF) was calculated using equation (1) [24]:

$$\boldsymbol{DF}\ (\%) = \frac{(\boldsymbol{Aromatic\ protons, H})/3}{(\boldsymbol{H1-G})/0.39} \qquad)$$

The average hydrodynamic diameter (d) and polydispersity index (PdI) of PDA particles were measured by Dynamic Light Scattering (DLS) using a Zetasizer Nano ZS (Malvern Instruments, UK). Atomic Force Microscopy (AFM) images of the PDA particles were acquired in air at room temperature using an AFM module (tapping mode) integrated into the neaSNOM system (Neaspec, Martinsried, Germany). Standard AFM tips coated with Pt/Ir (Arrow™ NCPt, NanoWorld, Neuchâtel, Switzerland), with a tip radius of less than 25 nm, were used for image acquisition.

2.3.2 Beads characterization

To determine the rehydration behavior, lyophilized beads were weighed (W_d) and individually incubated in distilled water at 37 °C. The swollen weight (W_s) was measured by removing the samples from water at predetermined time intervals, gently blotting them with filter paper and then weighing them. The swelling degree (SD) was calculated using the following equation:

$$\boldsymbol{SD = \frac{W_s - W_d}{W_d} \times 100} \quad (2)$$

The maximum swelling degree (MSD %) for each sample was calculated in the same manner, based on the wet weight at equilibrium. The results were reported as average values, with error bars representing the standard deviation. Beads' gel fraction was calculated with the following equation where W_f is the final mass of the lyophilized beads after maintaining them in distilled water at 37ºC for 3 days and W_i is the initial dry mass of the samples:

$$\mathbf{GF = \frac{W_f}{W_i} \times 100} \quad (3)$$

The resulting composite beads were morphologically investigated using scanning electron microscopy (SEM) with Zeiss EVO MA15 equipment with the following characteristics: resolution of 3 nm at an accelerating voltage of 30 kV (under high vacuum, using secondary electrons-SE) and a diameter of the field of view of 6 mm at a working distance of 8.55 mm. Finally, the beads were assessed in terms of cellular activity using indirect tests on 3T3 mouse fibroblasts. Cells were allowed to adhere to the substrate of a 24 wells culture plate and maintained in 1 mL per well of specific culture medium until reaching approximately 80% confluence. To assess the cytotoxic effect of the particles, each sample was immersed and incubated in 3 mL of Dulbecco's Modified Eagle Medium for 24 h under standard culture conditions. The extracts obtained from each material composition were collected and kept at 37°C. Once the cells reached 80% confluence, the culture medium was replaced with 1 mL per well of each collected extract. The cells were then incubated with these extracts for an additional 24 h under standard conditions of 37°C, 5% CO_2, and appropriate humidity. A Live/Dead fluorescent staining kit was used to qualitatively assess the ratio of viable to dead cells. Viable cells stained green and dead cells-stained red were examined using a Zeiss 710 confocal microscope, and the images were analyzed with Zeiss Zen software. Additionally, MTT and LDH test were performed using standard assay kits.

2.4 Results and discussion

Alg-DA synthesis. The coupling of dopamine on alginate's backbone was performed using an EDC/NHS system [25]. FTIR spectra of alginate (Alg), DA and Alg-DA were recorded to identify characteristic functional groups and to confirm

the modifications achieved (Fig. 1a). A broad and intense band observed at 3212 cm^{-1} in both the Alg and Alg-DA spectra that corresponds to the stretching vibration of the −OH groups. Both spectra also display the C−O−C stretching vibration at 1024 cm^{-1} and a characteristic alginate peak around 885 cm^{-1} specific to β-1,4-glycosidic bond [26]. Notably, the Alg-DA spectrum shows an additional absorption peak at 1080 cm^{-1}, which can be attributed to C–N amine stretching, indicating successful acylation and the formation of covalent bonds between alginate and dopamine [27]. Additionally, the presence of an absorption maximum at ~2900 nm^{-1} can be attributed to the vibration of the CH_2 group in dopamine, demonstrating that this molecule is present in the Alg-DA material [28]. UV-Vis spectroscopy studies revealed the successful grafting of dopamine on alginate, the spectra in Fig. 1b showing a strong peak around 280 nm, characteristic of dopamine [29]. Fig. 1c shows the ^{1}H-NMR spectra of modified and un-modified alginate. Upon analysis, new signals emerge in the Alg-DA spectrum with respect to the Alg spectrum, at 6.92 ppm, 6.86 ppm and 6.77 ppm corresponding to the aromatic protons of dopamine; together with 3.23 and 2.88 ppm signals attributed to the -CH_2-CH_2-NH_2 groups of dopamine, confirm the successful reaction of DA with the -COO- of Alg [30]. The DF was also calculated and established at 15%.

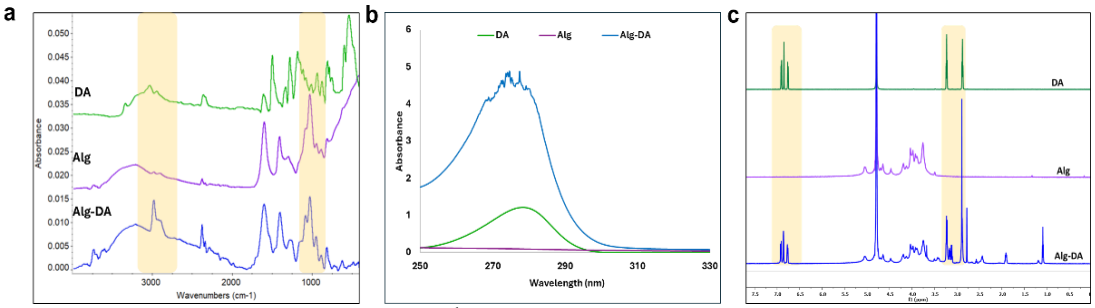

Fig. 1 a) FTIR, b) UV-Vis and c) ^{1}H-RMN spectra of pristine Alg, DA and Alg-DA

PDA particles synthesis. FTIR spectroscopy was used to compare the chemical structure of DA and PDA before and after the polymerization process (Fig. 2a). The DA spectrum displayed well-defined bands at 3035 and 2956 cm^{-1}, attributed to the stretching vibrations of O–H groups in the aromatic ring, indicating a relatively simple, unpolymerized molecular structure. Additionally, bands observed at 1331, 1277, and 1180 cm^{-1} were associated with C–O–H vibrations, C–O symmetric stretching, and C–C vibrations within the aromatic chain [31]. Conversely, the FTIR spectrum of PDA shows structural changes, beginning with a broad and intense band between 3000–3600 cm^{-1}, attributed to overlapping N–H and O–H stretching vibrations. This suggests the formation of an extensive hydrogen-bonding network following dopamine's auto-oxidation and polymerization. Moreover, the sharp absorption maximum of the benzene ring in DA, observed at 1496 cm^{-1}, is replaced in PDA by broader signals at 1575 and 1507

cm^{-1}, associated with the C=C vibrations of the indole structure, which results from dopamine cyclization. These changes confirm the successful formation of PDA and the transition from a simple molecule with well-defined functional groups to a complex macromolecular network rich in polar groups [17]. To determine the particle size distribution, a PDA solution was prepared by dispersing the particles in distilled water and was analyzed by DLS. The results showed an average particle size of 534 nm, with a polydispersity index of 0.306, indicating a relatively broad size distribution (Fig. 2b). AFM was used to analyze the morphology and size distribution of the PDA particles. To the best of our knowledge, no other AFM-assisted topography studies of already synthesized PDA particles were reported in literature, most research being focused on PDA coatings. The AFM images revealed a uniform particle distribution, confirming the DLS results, namely the formation of spherical structures with sizes around 500 nm (Fig. 2c).

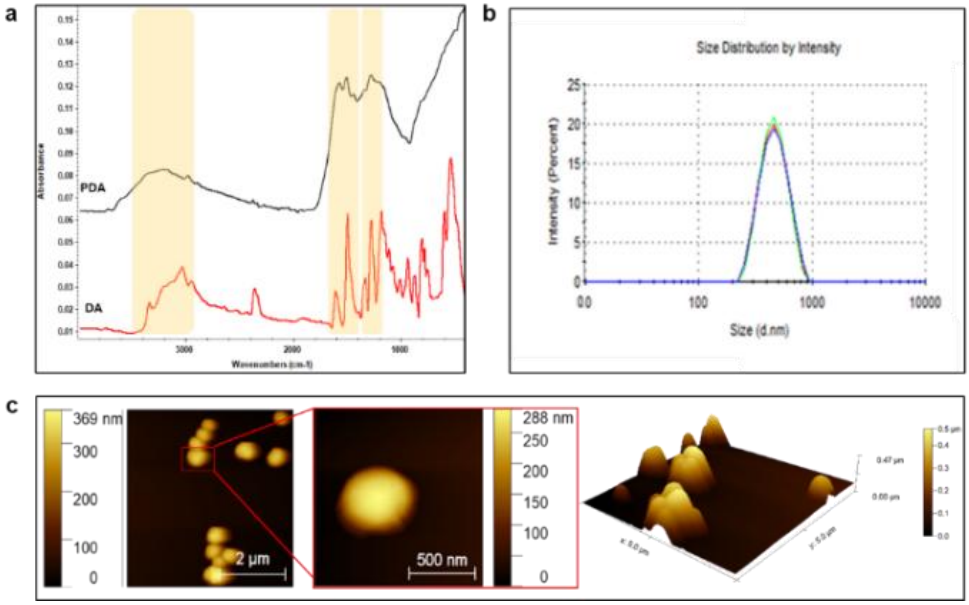

Fig. 2 a) FTIR spectra of DA and PDA, b) hydrodynamic diameter distribution diagram determined by DLS and c) AFM images of the PDA particles

Characterization of PDA-containing alginate-pectin calcium composite beads

The polymeric beads were obtained through injection-gelation method controlled by a syringe pump, therefore, at macroscale, homogeneity is observed in terms of size and shape in specific groups, as evidenced in Fig. 3.

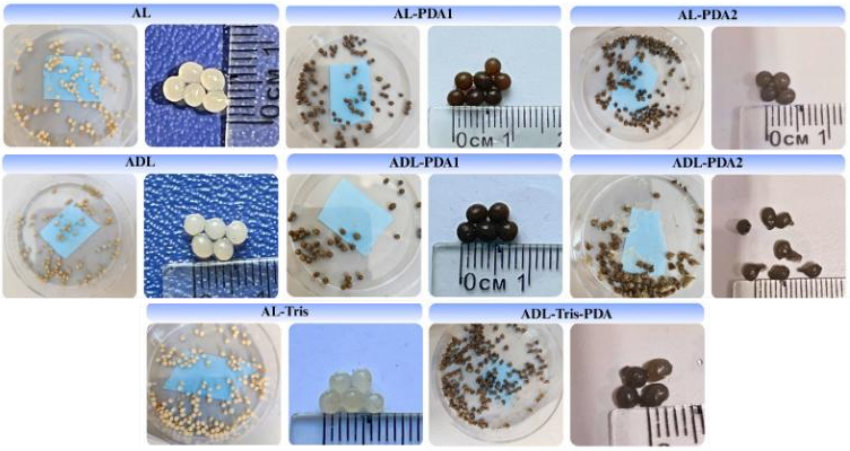

Fig. 3 Overview of bead appearance at the macroscopic level, dried and swollen at equilibrium

Except for ADL-PDA2 and ADL-Tris-PDA, all beads have a spherical shape with a diameter around 2-3 mm. The tear shape of the two samples can result from the following reasons: an increased viscosity of the solution and the addition of Tris along with the fact that, upon departing the needle, the droplet cannot achieve a complete spherical shape before contacting the $CaCl_2$ solution if the surface tension of the polymeric mix is considerably lower than that of water [32]. In terms of color, it is observed that the samples containing PDA gained a characteristic dark-brown color, confirming once more the formation of the compound.

Rehydration behavior

To simulate physiological conditions, the samples were incubated in an aqueous medium at 37°C, corresponding to human body temperature. The control samples exhibit moderate swelling behavior (Fig. 4a). The swelling value for AL is slightly higher than that for ALD, suggesting that the modification of alginate leads to a denser network that absorbs less liquid [33]. When PDA is incorporated into the internal structure (in AL-PDA1 and ADL-PDA1), the swelling values slightly decrease compared to controls (Fig. 4b). This reduction indicates a more compact structure or additional interactions between polymer chains, likely due to the reinforcing effect of PDA within the gel matrix. This suggests that PDA contributes to increased stability but restricts chain mobility and, consequently, their ability to expand in the presence of water [19]. Samples AL-PDA2 and ADL-PDA2 (Fig. 4c), which were treated with DA to form an external PDA coating, show very high swelling values, significantly greater than those of the other samples. This indicates a loosely crosslinked internal network with many free spaces between polymer chains. It is possible that, during DA treatment in aqueous media, the internal

structure of the hydrogel underwent partial degradation or destabilization of the network, leading to a loss of three-dimensional structural integrity. Samples AL-Tris and ADL-Tris-PDA (Fig. 4d) exhibit a relatively balanced swelling behavior. This moderate swelling range may be considered the most suitable for biomedical applications, as it indicates a polymer network that is stable enough to maintain structural integrity while also allowing sufficient nutrient diffusion, which is essential for cell interaction. The results obtained after 24 hours of hydration reveal distinct behaviors depending on the composition and treatment of the samples (Fig. 4e). Sample AL shows a modest swelling capacity, while the introduction of DA functionalities into alginate (ADL) leads to a doubling of water retention, suggesting a more flexible network with increased affinity for water. The addition of PDA particles into the composite matrix (AL-PDA2 and ADL-PDA2) results in a moderate increase compared to AL. However, the swelling values do not exceed those of ADL, indicating that the bulk incorporation of PDA does not provide clear benefits in the presence of Alg-DA and may slightly restrict network expansion [34]. In contrast, the use of Tris buffer solution (AL-Tris and ADL-Tris-PDA) has a much more pronounced impact on the swelling degree. AL-Tris, containing native alginate, shows a substantial increase compared to AL, while ADL-Tris-PDA, formulated with Alg-DA, exhibits the highest hydration level among all samples. In the case of ADL-PDA2, the swelling degree reaches a very high level (~5000%), suggesting that the internal network was likely destabilized or partially disrupted, thus promoting excessive water uptake.

Gel fraction

The gel fraction is used to evaluate the degree of crosslinking of polymeric materials after 3 days of immersion in distilled water at 37ºC (Fig. 4f).

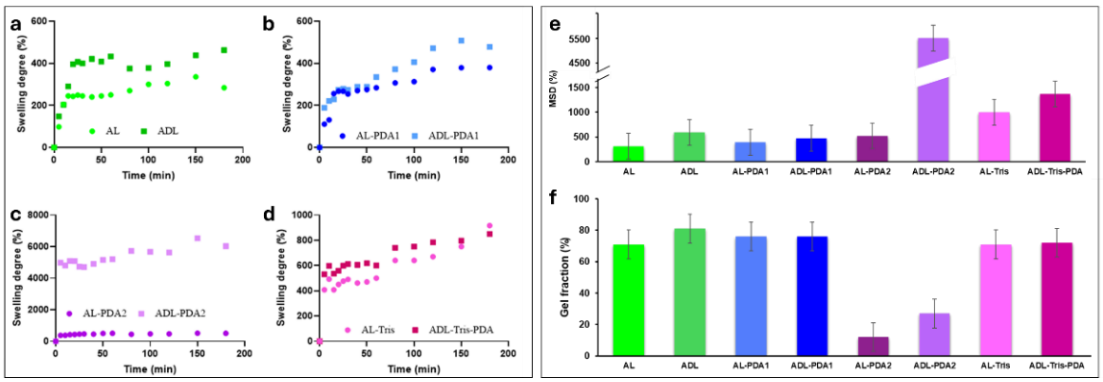

Fig. 4 Rehydration kinetics of a) AL, ADL; b) AL-PDA1, ADL-PDA1, c) AL-PDA2, ADL-PDA2; d) AL-Tris, ADL-Tris-PDA e) MSD at equilibrium; f) Quantification of the insoluble polymer fraction

Samples AL and ADL exhibit high gel fraction values, around 70–80%. These results reflect a well-crosslinked, stable network with a well-formed three-dimensional structure. The higher value recorded for ADL suggests that the chemical modification of alginate through dopamine incorporation enhances the ability to form interchain bonds, resulting in a denser network. Samples AL-PDA1 and ADL-PDA1, which contain PDA blended in the matrix, maintain high gel fraction values similar to those of AL and ADL. This indicates that the integration of PDA into the composite matrix does not negatively affect the crosslinking process; on the contrary, its presence may promote the formation of additional hydrogen bonds or π–π interactions, contributing to network stabilization [35]. In contrast, samples AL-PDA2 and ADL-PDA2, which were subjected to a surface coating treatment with PDA, show the lowest gel fraction values. In particular, AL-PDA2 samples, which contain native alginate, display a significantly reduced value, indicating a poorly stabilized network in which a large portion of the material remains uncrosslinked and susceptible to dissolution. ADL-PDA2, which contains Alg-DA, shows a slight improvement, but still falls short of the higher values observed in the other samples. Although PDA forms a protective surface layer, this does not significantly contribute to internal stability. Samples AL-Tris and ADL-Tris-PDA show a return to high gel fraction values, comparable to those of the initial samples. This result confirms that the alkaline pH generated by Tris does not compromise the crosslinking process and supports the formation of a stable and uniform network.

Morphological analysis with SEM

The obtained SEM images provide a detailed characterization of the porous architecture and the distribution of the components forming the spheres (Fig. 5). All samples are analyzed using two images, showing both the external surface and the internal structure after fracturing the spheres. Generally, it is observed that the surface of the samples is dense with no microporosity. However, unlike other studies in which it was reported that the shape of beads was wrinkled and exhibited a very collapsed and heterogenous surface, in our case, the beads remained spherical [36]. AL exhibits a porous morphology with thin walls and a random distribution of pores. The surface images reveal no evident aggregates, indicating good compositional homogeneity. In the fractured cross-section, a high porosity with an interconnected network is observed, suggesting a loosely crosslinked structure formed by Alg and LMP. For ADL, the surface appears similar to AL, indicating optimal interaction between components. The internal section shows smaller pores and a denser structure, confirming an increased crosslinking between Alg-DA and LMP. AL-PDA1 shows visible PDA particles that are distributed deep within the interior, and smaller pores alongside a more compact structure. The size of the particles within the internal matrix ranges between 200 and 400 nm, in accordance with the dimensions resulted from DLS and AFM investigations. In ADL-PDA1

the surface becomes denser and more uniform while PDA particles appear more evenly distributed across the matrix. Alg-DA contributes to better dispersion of PDA, and the internal images confirm an improved distribution of particles within the polymer network. Smaller pores and a consolidated structure indicate a high degree of crosslinking due to the synergy between Alg-DA and PDA. AL-PDA2 exhibits a PDA-coated surface that reduces pore size and gives a smooth and uniform appearance, PDA nanoparticles with diameters between 50 and 120 nm being visible. Notably, in situ precipitation of PDA yields smaller particles compared to the approach using pre-synthesized PDA. At higher magnification, fine details of the PDA layer are revealed, showing a homogeneous coating on the polymer matrix. Similarly, ADL-PDA2 shows a more homogeneous surface, but the nanoparticles are no longer individualized on the surface.

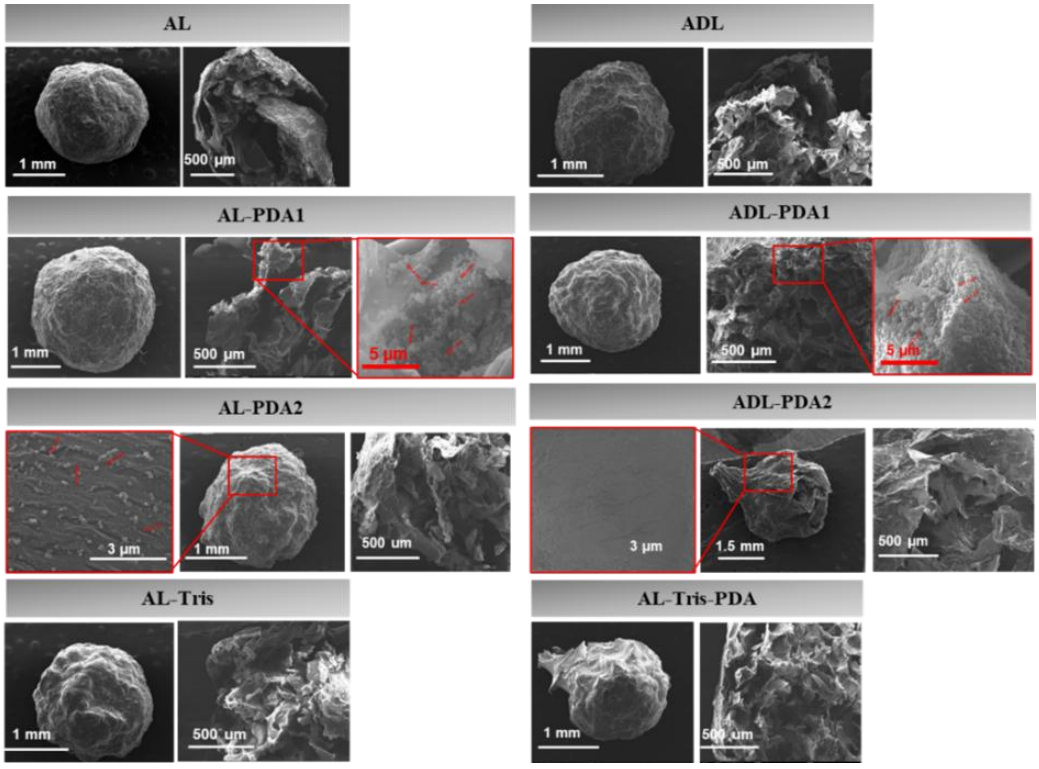

Fig. 5 SEM micrographs of the polysaccharidic beads: surface topography and internal architecture

However, it seems that the prolonged exposure of the ADL-PDA2 beads to DA-containing Tris solution led to more fragile beads that ruptured during lyophilization. For AL-Tris, the surface becomes smoother and more compact, and the inner-section images reveal a dense network. Sample ADL-Tris-PDA presents the densest and most uniform surface, without visible porosity while cross-sectional visualization confirms a fully consolidated structure with no evident aggregates

resulted from PDA precipitation. However, similar to ADL-PDA2, the sphericity of the samples was affected by the extensive immersion in Tris solution.

In vitro biocompatibility evaluation

Indirect biocompatibility assays were performed in order to investigate cellular viability of a fibroblast's culture and any possible cytotoxic effects of the polysaccharidic beads (Fig. 6). MTT assay was used to quantify cellular metabolic activity after 24h exposure to materials' extracts condition media (Fig. 6a). Minor differences in absorbance values were observed between samples ALD, AL-PDA2 and AL-Tris, without significant changes in metabolic activity, suggesting overall good biocompatibility.

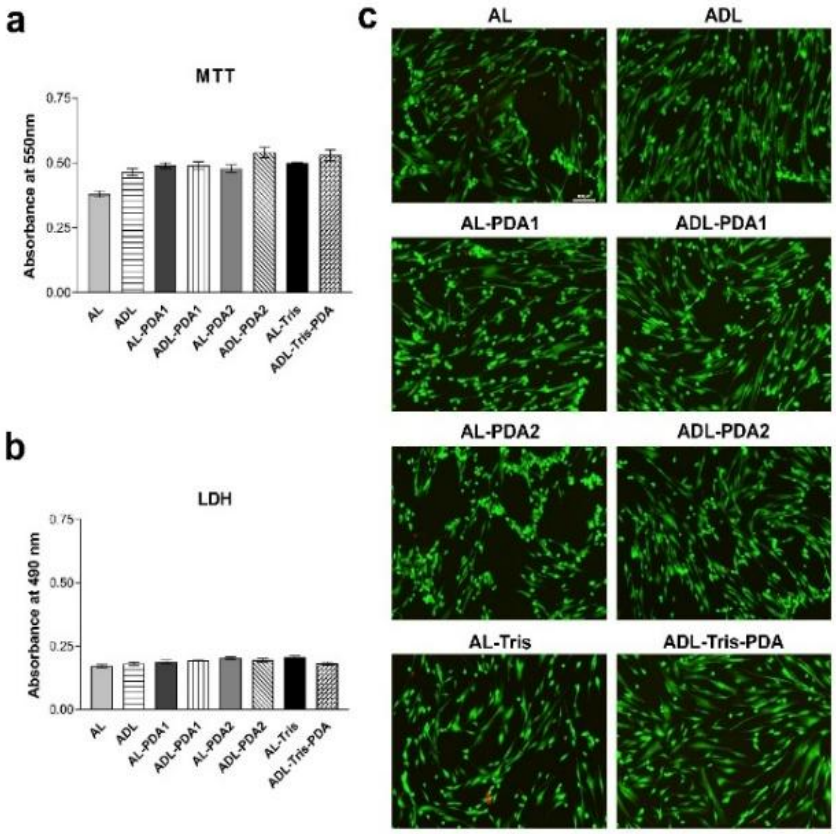

Fig. 6 a) MTT assay results; b) LDH assay results; c) Live/Dead staining: live cells are represented in green using calcein and dead cells' nuclei are stained in red with ethidium bromide.

However, notable variations in metabolic activity were detected among the samples, especially between AL and the other formulations. Specifically, sample AL showed reduced viability, which may be attributed to the absence of additional

bioactive groups that promote cell adhesion. Samples AL-PDA1 and ADL-PDA1 exhibited higher viability compared to formulations AL and ALD, confirming the positive contribution of PDA to the cellular response, possibly by mimicking natural adhesion proteins. Sample ADL-PDA2 showed higher values than AL-PDA2, indicating that the presence of PDA both on the surface and within the internal composition of the material may better support cellular proliferation. Additionally, similar behavior was observed for the AL-Tris and ADL-Tris-PDA compositions, further confirming this hypothesis. Moreover, promising results were obtained after assessing compositions' cytotoxic profile using LDH assay. As shown in Fig. 6b, all samples exhibited low absorbance values at 490 nm, indicating a reduced release of LDH into the culture medium and, consequently, low cytotoxicity. This reflects good cellular compatibility of the tested materials, without significant damage to the integrity of the cell membrane. Live/Staining was then performed in order to observe the population of live and dead cells after the exposure of fibroblast culture to polysaccharidic beads' extracts for 24h (Fig. 6c). Samples ADL, ADL-PDA1, and ADL-Tris-PDA exhibited good to excellent biocompatibility, characterized by high viability and extended fibroblastic morphology and relatively few dead cells' nuclei, suggesting positive effects of these materials' extracts towards the fibroblasts' culture. Among these, ADL-Tris-PDA showed the best performance with dense, healthy cells that display an elongated morphology and no signs of toxic effects. Samples AL, AL-PDA1, ADL-PDA2 and AL-Tris showed moderate results with a significant proportion of cells adopting a rounded shape, possibly indicating a more stressful environment. These samples also exhibited more red-stained nuclei of dead cells. Further, for the AL-PDA2 samples, an interesting behavior of fibroblasts was observed, with an increase proportion of rounded cells that seem to form multiple aggregates, an indicator of stressful conditions.

3. Conclusions

Several compositions based on PDA-supplemented alginate-pectin polymeric matrices were designed and tested. The injection-gelation approach was employed to make macroscopically sized beads with structural and functional properties. Understanding how PDA inclusion impacts the beads' function was our primary goal to maximize their potential as cell encapsulation and delivery platforms. It was shown that including PDA into the alginate-pectin matrix had a significant influence on the beads' macroscopic appearance, internal microstructure, and physical integrity. Most samples preserved their spherical form, with the exception of ADL-PDA2 and ADL-Tris-PDA, demonstrating that extended exposure to moderate alkaline aqueous environments might alter polymeric matrices containing Alg-DA. Except for ADL-PDA2, all samples are resistant to

fragmentation during handling and processing and have appropriate mechanical strength. Adding PDA to the hydrogel network boosted crosslinking density, as seen by slightly higher gel fraction values. This is probably because PDA may increase crosslinking sites through interactions with catechol and hydrogen bonding. The PDA inclusion strategy altered swelling behavior, which is another important cell encapsulation matrix property. Reduced swelling can maintain volume stability and bead integrity, but it can also hinder the passage of nutrients, oxygen, and metabolic waste-all of which are required for cell survival. This underscores how important formulation optimization is in achieving the right combination of stability and functionality. AL-Tris and ADL-Tris-PDA exhibit the best swelling properties among the samples, with levels sufficient to support diffusion and cell proliferation. Morphological tests show that all samples have a porous internal architecture, with AL-Tris and ADL-Tris-PDA revealing a somewhat denser network that does not appear to inhibit swelling, suggesting that the polymeric matrix is relatively robust and resistant to degradation while remaining flexible. This is corroborated by preliminary biocompatibility studies, which found that AL-Tris and ADL-Tris-PDA performed best in terms of cell survival, adhesion, and proliferation. However, there are still a number of unanswered questions and potential paths forward. First, to evaluate the behavior of PDA-modified beads under dynamic biological settings, such as enzymatic degradation and immunological response, long-term *in vitro* and *in vivo* stability experiments are required. Second, further research should be done on how PDA inclusion affects the phenotypic, function, and behavior of encapsulated cells. Lastly, progressing from laboratory research to therapeutic applications will require increasing the production process and evaluating batch-to-batch consistency. To sum up, our study shows a reliable and scalable method for creating functional macroscopic hydrogel beads using polydopamine-supplemented alginate-pectin matrices. For creating beads with precisely regulated size and composition, the injection-gelation process proven to be a dependable and adjustable platform. These results offer important information for the logical development of next-generation hydrogel systems intended for use in biomedical settings, including cell encapsulation.

REFERENCES

[1] T. Liu et al., “Aqueous two-phase emulsions-templated tailorable porous alginate beads for 3D cell culture,” Carbohydr. Polym., vol. 258, Apr. 2021, doi: 10.1016/j.carbpol.2021.117702.

[2] L. Gasperini, J. F. Mano, and R. L. Reis, “Natural polymers for the microencapsulation of cells,” Nov. 06, 2014, Royal Society of London. doi: 10.1098/rsif.2014.0817.

[3] T. Andersen, P. Auk-Emblem, and M. Dornish, “3D Cell Culture in Alginate Hydrogels,” Microarrays, vol. 4, no. 2, pp. 133–161, Mar. 2015, doi: 10.3390/microarrays4020133.

[4] L. Sun et al., “Novel konjac glucomannan microcarriers for anchorage-dependent animal cell culture,” Biochem. Eng. J., vol. 96, pp. 46–54, Apr. 2015, doi: 10.1016/j.bej.2014.12.012.

[5] R. A. de Carvalho, G. Veronese, A. J. F. Carvalho, E. Barbu, A. C. Amaral, and E. Trovatti, “The potential of TEMPO-oxidized nanofibrillar cellulose beads for cell delivery applications,” Cellulose, vol. 23, no. 6, pp. 3399–3405, Dec. 2016, doi: 10.1007/s10570-016-1063-2.

[6] B. Alallam, M. K. Oo, W. N. Ibrahim, and A. A. Doolaanea, “3D culture of cancer cells in alginate hydrogel beads as an effective technique for emergency cell storage and transportation in the pandemic era,” J. Cell. Mol. Med., vol. 26, no. 1, pp. 235–238, Jan. 2022, doi: 10.1111/jcmm.17078.

[7] I. Veernala, P. Roopmani, R. Singh, U. Hasan, and J. Giri, “Cell encapsulated and microenvironment modulating microbeads containing alginate hydrogel system for bone tissue engineering,” Prog. Biomater., vol. 10, no. 2, pp. 131–150, Jun. 2021, doi: 10.1007/s40204-021-00158-3.

[8] H. Samimi et al., “Alginate-based 3D cell culture technique to evaluate the half-maximal inhibitory concentration: an in vitro model of anticancer drug study for anaplastic thyroid carcinoma,” Thyroid Res., vol. 14, no. 1, Dec. 2021, doi: 10.1186/s13044-021-00118-w.

[9] S. Hu et al., “An immune regulatory 3D-printed alginate-pectin construct for immunoisolation of insulin producing β-cells,” Materials Science and Engineering C, vol. 123, Apr. 2021, doi: 10.1016/j.msec.2021.112009.

[10] J. A. Rowley, G. Madlambayan, and D. J. Mooney, “Alginate hydrogels as synthetic extracellular matrix materials,” 1999.

[11] S. S. Ho, A. T. Keown, B. Addison, and J. K. Leach, “Cell Migration and Bone Formation from Mesenchymal Stem Cell Spheroids in Alginate Hydrogels Are Regulated by Adhesive Ligand Density,” Biomacromolecules, vol. 18, no. 12, pp. 4331–4340, Dec. 2017, doi: 10.1021/acs.biomac.7b01366.

[12] S. K. Madhurakkat Perikamana et al., “Materials from Mussel-Inspired Chemistry for Cell and Tissue Engineering Applications,” Sep. 14, 2015, American Chemical Society. doi: 10.1021/acs.biomac.5b00852.

[13] M. Li, Y. Xuan, W. Zhang, S. Zhang, and J. An, “Polydopamine-containing nano-systems for cancer multi-mode diagnoses and therapies: A review,” Aug. 30, 2023, Elsevier B.V. doi: 10.1016/j.ijbiomac.2023.125826.

[14] J. Lu et al., “Polydopamine-Based Nanoparticles for Photothermal Therapy/Chemotherapy and their Synergistic Therapy with Autophagy Inhibitor to Promote Antitumor Treatment,” Apr. 01, 2021, John Wiley and Sons Inc. doi: 10.1002/tcr.202000170.

[15] Z. Deng et al., “Biofunction of Polydopamine Coating in Stem Cell Culture,” ACS Appl. Mater. Interfaces, vol. 13, no. 9, pp. 10748–10759, Mar. 2021, doi: 10.1021/acsami.0c22565.

[16] D. H. Yang, S. Jung, J. Y. Kim, and N. Y. Lee, “Fabrication of a Cell-Friendly Poly(dimethylsiloxane) Culture Surface via Polydopamine Coating,” Micromachines (Basel)., vol. 13, no. 7, Jul. 2022, doi: 10.3390/mi13071122.

[17] B. Gao et al., “Methods to prepare dopamine/polydopamine modified alginate hydrogels and their special improved properties for drug delivery,” Eur. Polym. J., vol. 110, pp. 192–201, Jan. 2019, doi: 10.1016/j.eurpolymj.2018.11.025.

[18] S. Zhang, K. Xu, M. A. Darabi, Q. Yuan, and M. Xing, “Mussel-inspired alginate gel promoting the osteogenic differentiation of mesenchymal stem cells and anti-infection,” Materials Science and Engineering C, vol. 69, pp. 496–504, Dec. 2016, doi: 10.1016/j.msec.2016.06.044.

[19] B. Gao et al., "Methods to prepare dopamine/polydopamine modified alginate hydrogels and their special improved properties for drug delivery," Eur. Polym. J., vol. 110, pp. 192–201, Jan. 2019, doi: 10.1016/j.eurpolymj.2018.11.025.

[20] J. Shen, D. Shi, L. Dong, Z. Zhang, X. Li, and M. Chen, "Fabrication of polydopamine nanoparticles knotted alginate scaffolds and their properties," J. Biomed. Mater. Res. A, vol. 106, no. 12, pp. 3255–3266, Dec. 2018, doi: 10.1002/jbm.a.36524.

[21] Z. Li, Y. Geng, K. Bu, Z. Chen, K. Xu, and C. Zhu, "Construction of a pectin/sodium alginate composite hydrogel delivery system for improving the bioaccessibility of phycocyanin," Int. J. Biol. Macromol., vol. 269, Jun. 2024, doi: 10.1016/j.ijbiomac.2024.131969.

[22] B. Chen, L. Huang, R. Ma, and Y. Luo, "3D printed hollow channeled hydrogel scaffolds with antibacterial and wound healing activities," Biomedical Materials (Bristol), vol. 18, no. 4, Jul. 2023, doi: 10.1088/1748-605X/acd977.

[23] A. I. Cernencu et al., "Bioinspired 3D printable pectin-nanocellulose ink formulations," Carbohydr. Polym., vol. 220, no. January, pp. 12–21, 2019, doi: 10.1016/j.carbpol.2019.05.026.

[24] F. Scognamiglio et al., "Enhanced bioadhesivity of dopamine-functionalized polysaccharidic membranes for general surgery applications," Acta Biomater., vol. 44, pp. 232–242, Oct. 2016, doi: 10.1016/j.actbio.2016.08.017.

[25] X. Wang, Z. Jiang, J. Shi, C. Zhang, W. Zhang, and H. Wu, "Dopamine-modified alginate beads reinforced by cross-linking via titanium coordination or self-polymerization and its application in enzyme immobilization," Ind. Eng. Chem. Res., vol. 52, no. 42, pp. 14828–14836, Oct. 2013, doi: 10.1021/ie401239e.

[26] X. Zhang et al., "Structural and Physical Properties of Alginate Pretreated by High-Pressure Homogenization," Polymers (Basel)., vol. 15, no. 15, Aug. 2023, doi: 10.3390/polym15153225.

[27] P. Li, Y. Li, R. Fu, Z. Duan, C. Zhu, and D. Fan, "NIR- and pH-responsive injectable nanocomposite alginate-graft-dopamine hydrogel for melanoma suppression and wound repair," Carbohydr. Polym., vol. 314, Aug. 2023, doi: 10.1016/j.carbpol.2023.120899.

[28] T. Yadav and V. Mukherjee, "Interpretation of IR and Raman spectra of dopamine neurotransmitter and effect of hydrogen bond in HCl," J. Mol. Struct., vol. 1160, pp. 256–270, May 2018, doi: 10.1016/j.molstruc.2018.01.066.

[29] J. Hou, C. Li, Y. Guan, Y. Zhang, and X. X. Zhu, "Enzymatically crosslinked alginate hydrogels with improved adhesion properties," Polym. Chem., vol. 6, no. 12, pp. 2204–2213, Mar. 2015, doi: 10.1039/c4py01757a.

[30] C. Lee et al., "Bioinspired, calcium-free alginate hydrogels with tunable physical and mechanical properties and improved biocompatibility," Biomacromolecules, vol. 14, no. 6, pp. 2004–2013, Jun. 2013, doi: 10.1021/bm400352d.

[31] X. Wen et al., "Constructing novel fiber reinforced plastic (FRP) composites through a biomimetic approach: Connecting glass fiber with nanosized boron nitride by polydopamine coating," J. Nanomater., vol. 2013, 2013, doi: 10.1155/2013/470583.

[32] B. B. Lee, P. Ravindra, and E. S. Chan, "Size and shape of calcium alginate beads produced by extrusion dripping," Oct. 2013. doi: 10.1002/ceat.201300230.

[33] J. Chi et al., "Novel dopamine-modified oxidized sodium alginate hydrogels promote angiogenesis and accelerate healing of chronic diabetic wounds," Int. J. Biol. Macromol., vol. 203, pp. 492–504, Apr. 2022, doi: 10.1016/j.ijbiomac.2022.01.153.

[34] M. Han, Z. Wang, Z. Xie, M. Hou, and Z. Gao, “Polydopamine-modified sodium alginate hydrogel for microplastics removal: Adsorption performance, characteristics, and kinetics,” Int. J. Biol. Macromol., vol. 297, Mar. 2025, doi: 10.1016/j.ijbiomac.2025.139947.

[35] M. Kashi, M. H. Nazarpak, J. Nourmohammadi, and F. Moztarzadeh, “Study the effect of different concentrations of polydopamine as a secure and bioactive crosslinker on dual crosslinking of oxidized alginate and gelatin wound dressings,” Int. J. Biol. Macromol., vol. 277, Oct. 2024, doi: 10.1016/j.ijbiomac.2024.134199.

[36] B. Wu, Y. Li, Y. Li, H. Li, L. Li, and Q. Xia, “Encapsulation of resveratrol-loaded Pickering emulsions in alginate/pectin hydrogel beads: Improved stability and modification of digestive behavior in the gastrointestinal tract,” Int. J. Biol. Macromol., vol. 222, pp. 337–347, Dec. 2022, doi: 10.1016/j.ijbiomac.2022.09.175.